Materials Today Communications 28 (2021) 102663

Contents lists available at ScienceDirect

Materials Today Communications

journal homepage: www.elsevier.com/locate/mtcomm

Thermal stability and decomposition kinetics of $NdNiO_{3-\delta}$ at 1 bar of O_2

A.A. Bassou [a], P.J. Machado [b], M.M. Gomes [b], B. Manjunath [b], R. Vilarinho [b], B. Silva [c], J. Oliveira [c], B. Almeida [c], A. Almeida [b], J.R. Fernandes [d], L.S. Fernandes [a], J. Agostinho Moreira [b], P.B. Tavares [a,*]

[a] Centro de Química-Vila Real, ECVA, Chemistry Department, Universidade de Trás-os-Montes e Alto Douro, 5000-801 Vila Real, Portugal
[b] IFIMUP, Departamento de Física e Astronomia da Faculdade de Ciências, Universidade do Porto, Rua do Campo Alegre s/n, 4169-007 Porto, Portugal
[c] CF-UM-UP, Departamento de Física, Universidade do Minho, Campus de Gualtar, 4710-057 Braga, Portugal
[d] Centro de Química-Vila Real, ECT, Physics Department, Universidade de Trás-os-Montes e Alto Douro, 5000-801 Vila Real, Portugal

ARTICLE INFO

Keywords:
A. Ceramics
A. Oxides
B. Phase transitions
C. X-ray diffraction
C. Raman spectroscopy

ABSTRACT

Despite the interest in rare-earth nickelates for applications, their processing under 1 bar of oxygen pressure is still challenging. In this work, we report the co-precipitation synthesis, thermal stability and thermally driven decomposition of $NdNiO_3$ phase, in order to determine the synthesis parameters towards a pure perovskite phase. We concluded that using a 1% molar excess of Nd during preparation and posterior annealing at around 900 °C at 1 bar of O_2 yields an almost pure $NdNiO_{3-\delta}$ phase (with a hexagonal Nd_2O_3 phase below 0.6% molar), with an oxygen deficiency of $\delta = 0.082 \pm 0.001$. The decomposition of the $NdNiO_{3-\delta}$ phase into $Nd_4Ni_3O_{10}$ and NiO was found to start above 900 °C. On further heating, above 1050 °C, the $Nd_4Ni_3O_{10}$ decomposes into Nd_2NiO_4 and NiO phases. Structural parameters and Raman spectra are provided for the $NdNiO_3$, $Nd_4Ni_3O_{10}$ and Nd_2NiO_4 compounds.

1. Introduction

Rare-earth nickelates $RNiO_3$ (RNO, R a trivalent rare-earth cation) are fascinating compounds due to their remarkable functional properties [1–4]. With the exception of $LaNiO_3$, which keeps the metallic rhombohedral *R*-3*c* symmetry down to 1.5 K, all RNO undergo a metallic-to-insulating phase transition (MIT) at T_{MI}, strongly dependent on the rare-earth cation size [5,6]. In RNO compounds with R = Lu to Sm, MIT is accompanied by a structural transition from the orthorhombic *Pnma* to the monoclinic $P2_1/n$ symmetry, and an isostructural antiferromagnetic phase transition occurring at the Néel temperature $T_N < T_{MI}$ [5,6]. In the cases of $NdNiO_3$ and $PrNiO_3$, these transitions occur at the same temperature, $T_{MI} = T_N$ [5,6]. The MIT has been interpreted as a consequence of the reduction and closing of the charge-transfer gap between O^{2-} and Ni^{3+} ions [7]. In this regard, oxygen stoichiometry is an important parameter to ensure functionality in RNO.

Applications of RNO have been more focused on thin films or heterostructured systems, where the epitaxial strain ensures the desired perovskite phase. The fabrication of such structures demands high quality targets, requiring large enough amount of material. This is not reasonable by using the high pressure synthesis technique that has been used to produce pure RNO phase [8]. Therefore, alternative chemical processing techniques have to be explored, while keeping the correct stoichiometry. The synthesis of RNO using conventional solid-state reaction or co-precipitation methods at 1 bar of oxygen pressure revealed themselves to be challenging techniques of obtaining high quality RNO ceramics. Except for $LaNiO_3$, RNO were synthesised following a wet chemical route under a 150 bar O_2 atmosphere and temperatures over 1000 °C [9]. In particular, the synthesis of $NdNiO_3$ performed at rather low temperature (650 °C) in 1 bar of oxygen pressure was reported [10–12]. However, these synthesis conditions yield oxygen deficient samples, and, consequently, different Ni oxidation states [10]. Samples synthesised under 50 bar of O_2 atmosphere at temperatures below 900 °C have moderated oxygen deficiency with $\delta = 0.06$ [10]. However, under 1 bar of O_2 atmosphere and a temperature of 800 °C, the oxygen deficiency in the $NdNiO_{3-\delta}$ phase is estimated to be close to $\delta = 0.29$ [10]. Yet, as δ increases the MIT critical temperature of $NdNiO_{3-\delta}$ decreases and the anomaly in the temperature dependence of the electric resistivity becomes less evident and eventually blurs for $\delta > 0.20$ [10].

Despite the highly requested interest in RNO for many applications, a detailed study of the best conditions for RNO synthesis under 1 bar of oxygen pressure and their thermal stability is still missing. In fact, both

* Corresponding author.
E-mail address: ptavares@utad.pt (P.B. Tavares).

https://doi.org/10.1016/j.mtcomm.2021.102663
Received 23 December 2020; Received in revised form 5 July 2021; Accepted 15 July 2021
Available online 18 July 2021

kinetic and thermodynamic considerations must be considered, when synthesising RNO compounds. To achieve low δ values in $NdNiO_{3-\delta}$, temperatures below 700 °C must be considered since oxygen content increases at lower temperatures [13]. However, lowering synthesis temperature can yield a disadvantageous slowing down of the phase formation kinetics, associated with lower ion diffusivity. The cooling rate of the samples also plays an important role in defining δ value; while high cooling rates from temperatures above 1000 °C yield high δ values, slow or very slow cooling rates in O_2 atmosphere decreases δ [13]. Moreover, a detailed study concerning the emergence of impurity phases is required to understand how they evolve whilst changing the annealing parameters [11].

In this work, we report the synthesis, thermal stability and the thermally driven decomposition of $NdNiO_3$ phase in pure oxygen atmosphere at 1 bar pressure. The detailed analysis of the obtained experimental results, using adequate techniques, will yield a comprehensive understanding of both the thermal stability and decomposition kinetics of $NdNiO_3$. It will be then possible to determine which synthesis parameters minimise the spurious phase formation, and effectively synthesise a pure perovskite $NdNiO_3$ phase. The oxygen non-stoichiometry of the prepared $NdNiO_3$ samples will also be addressed by a comprehensive analysis of the obtained resistivity and XPS results.

2. Material and methods

$NdNiO_{3-\delta}$ samples (hereafter referred as $NdNiO_3$ samples) were synthesised by co-precipitation method. Preliminary studies have shown that samples prepared with 1% molar excess of Nd as starting point lead to stoichiometric samples. This compensates the small loss of Nd due to $Nd(OH)_3$ solubility and Nd_2O_3 volatilisation (see more details in the S1 Section of Supplemental material). Briefly, $Nd(NO_3)_3{\cdot}6H_2O$ (Alfa Aesar 99.99%REO) and $Ni(NO_3)_2{\cdot}6H_2O$ (Alfa Aesar 99.9%) powders were dissolved in double distilled water. A solution of NaOH 1 M (Aldrich 99.99%) was added until pH = 12 was reached, and kept under strong stirring for 12 h. The solution was decanted and the precipitate was washed several times with water until no sodium was detected by flame-AAS in the washing water. After drying, the powder was calcinated in an alumina crucible at 500 °C for 2 h followed by grinding, pelletizing (13 mm diameter and 3 mm height) and thermal treatment at 650 °C in 1 bar of flowing O_2 (Gasin O_2 X50S, 20 mL/min) in a tubular oven for at least 120 h. The resulting pellets are black and shiny. This method avoids high-temperature treatments compared to solid state synthesis, eliminating intermediate regrinding stages. In addition, it avoids the use of more expensive reactants or the emission of pollutants into the atmosphere, as in the sol-gel process.

To study the thermal stability of the $NdNiO_3$ phase and its thermally-driven decomposition, several as-processed samples were annealed at different fixed temperatures, ranging from 650 °C up to 1200 °C, in 1 bar of flowing O_2 atmosphere for 12 h. In between those studies, an additional study of $NdNiO_3$ decomposition kinetics was performed at 950 °C using different time intervals (12 h, 20 h, 100 h and 120 h). Besides, a slow cool rate (2 °C/min) to room temperature was applied. Fig. 1 chronologically describes the annealing history of these two studies.

X-ray diffraction (XRD) patterns were recorded at room temperature after each annealing step, using a Panalytical MPD diffractometer equipped with a X′Celerator detector and secondary monochromator in Bragg–Bentano geometry. $CuK\alpha_{1,2}$ radiation, $\lambda_1 = 1.5406$ Å, $\lambda_2 = 1.5444$ Å, a step size of 0.017° and 100 s/step were used. Full Rietveld refinements were performed using PowderCell 2.4 and HighScore 4.8. Volume percentages from PowderCell were converted to weight percentages using the calculated density from each phase. Conversions to molar percentages were done using molar mass from each phase (see Section S2 of the Supplemental material). Lattice parameters, atomic and Wyckoff positions were obtained from the Rietveld refinements. Scanning Electron Microscopy (SEM) was performed using a FEI Quanta 400 with W filament and energy dispersive X-ray spectrometry (EDS) from EDAX.

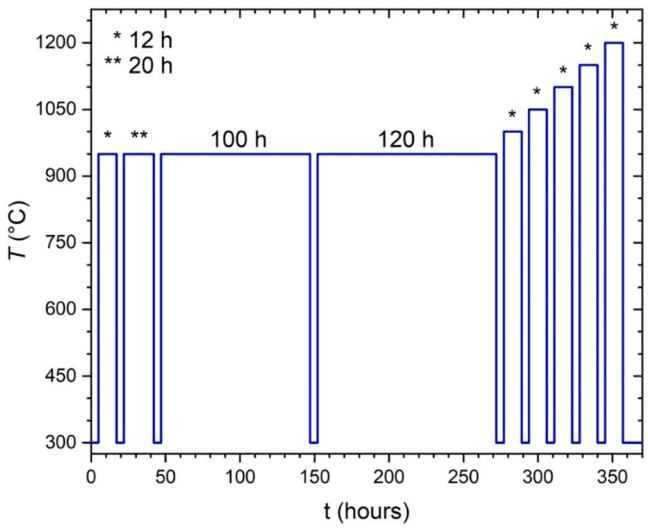

Fig. 1. Annealing history of the sample, above 900 °C. The sample was annealed at a fixed temperature followed by XRD measurements performed at room temperature. The sample was kept at 950 °C at different time intervals in order to study the decomposition kinetics of $NdNiO_3$.

The unpolarised micro-Raman spectra were recorded in a backscattering geometry at ambient conditions, using a 100× objective lens of a Leica microscope. The 633 nm He-Ne laser line was used for excitation and the scattered light was analysed by a Renishaw inVia Qontor spectrometer. The effect of the laser power on the Raman spectra was previously studied to prevent self-heating of the sample. In the as-processed samples, the Raman spectra, recorded at different surface sample regions (~ 1 μm^2 laser focus area), exhibit the same number of bands with similar spectral positions and relative intensities. This result provides experimental evidence of both the structural and chemical homogeneity of the samples. A sum of damped harmonic oscillators was fitted to the experimental spectra so that mode wavenumber and linewidth could be obtained [14].

The electrical resistivity measurements were performed in the temperature range of 120–300 K using the standard four-probe in-line technique. The temperature dependent measurements were made using a closed-cycle APD Cryogenics cryostat and controller, with a cooling \heating rate of 1 K/min. A current was then applied to the outer electrodes using the current source of a Keithley 617 electrometer and measured with a Tektronix DMM4040 Precision Multimeter. Voltage in the inner electrodes was measured with HP 34401A Precision Multimeter. The obtained resistance was then multiplied by the section area and divided by the electrode length to obtain the electrical resistivity. For the resistivity measurements, the samples were cut in a parallelepiped shape, the length (15.5 mm) being longer than the thickness/width (2 mm). Prior to the measurements, 4 in-line gold contacts were deposited on top of the samples to be used as electrodes. The contact diameters were 1 mm, separated by a 2 mm distance. The wires leading to the measurement equipment were glued to the contacts with air curing silver paste.

The X-ray photoelectron spectroscopy (XPS) analysis was performed using monochromatic Al-Kα radiation (1486.6 eV, operating at 15 kV) from a Kratos AXIS Ultra HSA, to obtain the oxidation states of each element. The effect of the electrical charge was corrected by the reference of the carbon peak C 1s (285 eV). The analysis of the spectra, recorded at two different sample surface positions, was performed with the CasaXPS software, fitting a Gaussian–Lorentzian peak shape with a Shirley type background subtraction.

3. Results and discussion

3.1. Morphological, chemical and structural characterisation

Fig. 2 shows a representative SEM image of a sample with nominal ratio of Nd/Ni = 1.01 which was prepared and treated at 650 °C in flowing O_2 for 240 h. The microstructure evidences a porous material (relative density around 70%) and near cubic geometric grains, with a mean grain size of 174 ± 22 nm. From EDS data, a ratio of Nd/Ni = 0.98 ± 0.03 was determined, pointing out to stoichiometric samples within the error of the EDS method.

The representative room temperature XRD pattern of $NdNiO_3$ sample, treated at 650 °C in 1 bar of flowing O_2 for 240 h, shown in Fig. 3, evidences the expected orthorhombic *Pnma* crystallographic phase, as reported by Hooda et al. [12]. The diffraction pattern also exhibits other features assigned to two secondary phases: hexagonal Nd_2O_3 [15] (1.1 vol%) and cubic Nd_2O_3 [16] (1.0 vol%). The lattice parameters obtained from the refinements are presented in Table 1, as well as the atomic and Wyckoff positions used from the published literature [12].

3.2. Thermal stability of phases

Representative room temperature XRD patterns of the samples after having undergone the annealing process, along with the JCPDS XRD patterns of $NdNiO_3$, $Nd_4Ni_3O_{10}$, Nd_2NiO_4 and NiO for comparison, are shown in Fig. 4. These last three phases are the resulting products of the thermally-driven decomposition of $NdNiO_3$ given by Equations [10]:

$$4NdNiO_3 \rightarrow Nd_4Ni_3O_{10} + NiO + \tfrac{1}{2}O_2 \quad (1)$$

$$Nd_4Ni_3O_{10} \rightarrow 2Nd_2NiO_4 + NiO + \tfrac{1}{2}O_2 \quad (2)$$

The atomic positions were refined by Rietveld analysis of the XRD patterns using the *Pnma* [12] and *Cmca* [17] space groups for $NdNiO_3$ and Nd_2NiO_4, respectively, while the $Nd_4Ni_3O_{10}$ crystallographic phase was refined using the $P2_1/a$ space group [18]. Figs. S2 and S3 in Section S2 of Supplemental material show the results of the Rietveld refinement for the $NdNiO_3$ samples during heat treatments in O_2 at different temperatures and $NdNiO_3$ samples during heat treatments at 950 °C in O_2 at different time intervals, respectively. The values regarding bond lengths and bond angles of $NdNiO_3$, Nd_2NiO_4 and $Nd_4Ni_3O_{10}$ obtained from the Rietveld analysis are presented in Table S1 in Supplemental material. The experimental lattice parameters and atomic positions are also given in Table 1. The obtained *a*, *b* and *c* lattice parameters can be compared with previously published ones, 5.379 Å, 7.602 Å, 5.410 Å for $NdNiO_3$ [12], 5.471 Å, 12.211 Å, 5.465 Å for Nd_2NiO_4 [17] and 5.3675 Å, 5.4548 Å, 27.433 Å, with a 90.312° monoclinic angle for $Nd_4Ni_3O_{10}$ [18]. The small differences observed between the here reported and published lattice parameters of $NdNiO_3$ are assigned to oxygen non-stoichiometry; i.e. $NdNiO_{3-\delta}$ as we will discuss later on. The differences in $Nd_4Ni_3O_{10}$ and Nd_2NiO_4 lattice parameters can be the result of an excess of NiO leading to small Ni-excess compounds.

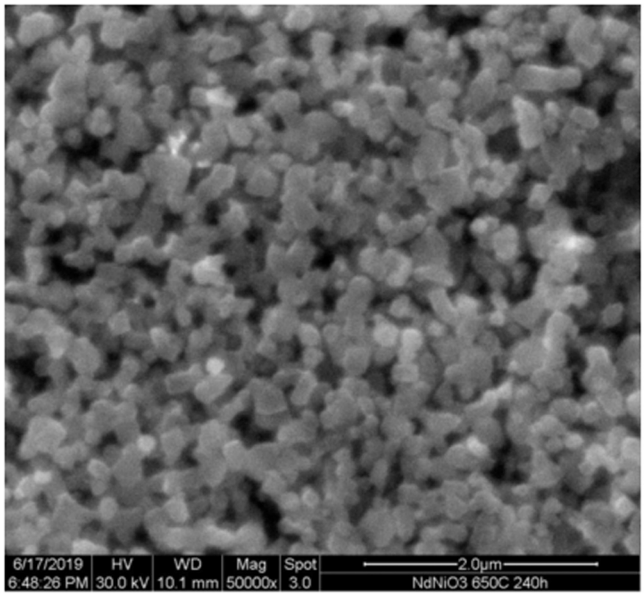

Fig. 2. Representative SEM image of $NdNiO_3$ sample, treated at 650 °C at 1 bar of flowing O_2 for 240 h.

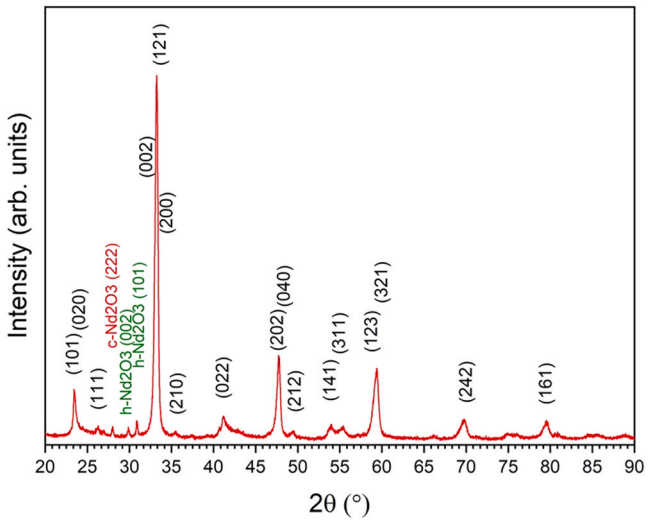

Fig. 3. Representative room temperature XRD pattern of $NdNiO_3$ sample treated at 650 °C in 1 bar of flowing O_2 for 240 h.

In Fig. 4, the XRD patterns for both samples annealed at 730 °C and 900 °C evidence just the presence of the $NdNiO_3$ perovskite phase. This phase starts to decompose as the annealing temperature increases, and then new phases emerge. The XRD patterns of the samples annealed at 1000 °C and 1150 °C reveal the presence of $Nd_4Ni_3O_{10}$ and Nd_2NiO_4, respectively. For these two annealing temperatures, we can clearly see the emergence of a new peak around $2\theta = 37°$, arising from the NiO phase. As we will see further ahead, the emergence of this phase is associated with the $NdNiO_3$ decomposition, as it is predicted by both Eqs. (1) and (2).

Fig. 5 shows the relative amounts (in molar percentage) of the different chemical phases obtained from the Rietveld refinement as a function of the annealing temperature. For annealing temperatures up to 900 °C (part A of Fig. 5), a $NdNiO_3$ phase is formed, but with 2% of Nd_2O_3 impurity (see inset of Fig. 5) which is likely to occur due to the small excess of Nd used in sample preparation. For annealing temperatures below 700 °C, a mixture of cubic and hexagonal Nd_2O_3 phases is observed, whereas for the sample annealed between 700 °C and 900 °C only hexagonal Nd_2O_3 is observed, whose molar percentage decreases and eventually vanishes around 900 °C. This is probably the result of a small loss of Nd due to volatilisation, which accounts for the correct sample stoichiometry. Hence, it may be concluded that the $NdNiO_3$ phase is stable at 1 bar of O_2 up to 900 °C. This result clearly evidences that a 1% excess of Nd during preparation and posterior annealing at around 900 °C creates an almost pure and stoichiometric $NdNiO_3$ phase. If any spurious phases happen to occur, their volume percentage is below the diffraction limit of the XRD apparatus, i.e. less than 0.5%.

Above 900 °C (see Part B of Fig. 5), $NdNiO_3$ starts to decompose into NiO and $Nd_4Ni_3O_{10}$, as described by Eq. (1). As the annealing temperature increases towards 1000 °C the relative amount of $NdNiO_3$ phase continuously decreases, and it completely disappears at 1000 °C. Note that at this temperature, the relative amounts of the different chemical

Table 1
Room temperature lattice parameters of $NdNiO_3$, $Nd_4Ni_3O_{10}$ and Nd_2NiO_4, obtained in this work. Atomic and Wyckoff positions (WP) from Refs. [12]. Standard settings are used.

$NdNiO_3$	
Space group	*Pnma* (62)
Lattice parameters	
a (Å)	5.398(1)
b (Å)	7.631(1)
c (Å)	5.450(1)
	Relative atomic pos. (WP; x,y,z)
Nd	4c; 0.5319, 0.25, 0.5065
Ni	4b; 0, 0, 0
O1	4c; 0.9577, 0.25, 0.4488
O2	8d; 0.7847, 0.4459, 0.7848
Nd_2NiO_4	
Space group	*Cmca* (64)
Lattice parameters	
a (Å)	5.369(1)
b (Å)	12.364(1)
c (Å)	5.447(1)
	Relative atomic pos. (WP; x,y,z)
Nd	8f; 0, 0.3632, 0.0150
Ni	4a; 0, 0, 0
O1	8e; 0.25, 0.0179, 0.25
O2	8f; 0, 0.3206, 0.437
$Nd_4Ni_3O_{10}$	
Space group	$P2_1/a$ (14)
Lattice parameters	
a (Å)	5.365(1)
b (Å)	5.440(1)
c (Å)	27.378(5)
β (°)	90.20(1)
	Relative atomic pos. (WP; x,y,z)
Nd1	4e; -0.016, 0.018, 0.3006
Nd2	4e; 0.508, 0.009, 0.8001
Nd3	4e; 0.04, 0.011, 0.4313
Nd4	4e; 0.514, -0.001, 0.9316
Ni1	2d; 0, 0.5, 0.5
Ni2	2a; 0, 0, 0
Ni3	4e; -0.014, 0.005, 0.1404
Ni4	4e; 0.501, 0.003, 0.6402
O1	4e; 0.297, 0.3, 0.4913
O2	4e; 0.267, 0.231, 0.9891
O3	4e; -0.003, 0.076, 0.069
O4	4e; 0.509, 0.074, 0.5694
O5	4e; 0.241, 0.242, 0.1492
O6	4e; 0.758, 0.239, 0.6516
O7	4e; -0.031, -0.051, 0.2167
O8	4e; 0.525, -0.061, 0.7166
O9	4e; 0.753, 0.249, 0.8715
O10	4e; 0.268, 0.26, 0.3657

phases could be somehow affected by the cumulative effect of the thermal treatment of the sample at 950 °C (see the annealing history of the sample in Fig. 1). At 1050 °C, the relative amount of $Nd_4Ni_3O_{10}$ reaches its maximum value. On further annealing temperature increase, the $Nd_4Ni_3O_{10}$ phase decomposes into the Nd_2NiO_4 one, according to Eq. (2).

It is worth emphasising that the amount of NiO phase monotonously increases with increasing annealing temperature, as this phase can be obtained from the decomposition of $NdNiO_3$ and $Nd_4Ni_3O_{10}$ phases. The sample annealed at 1200 °C has NiO and Nd_2NiO_4 phases only.

The $NdNiO_3$ phase is connected to the Nd_2O_3 and NiO phases, meaning that non-stoichiometric samples will lead to the appearance of these secondary phases [10,12]. Consequently, $NdNiO_3$ samples must be prepared with extreme care. At temperatures above 800 °C, due to Nd volatilisation, losses of Nd_2O_3 must be compensated or eliminated by appropriate experimental procedures, otherwise NiO secondary phase

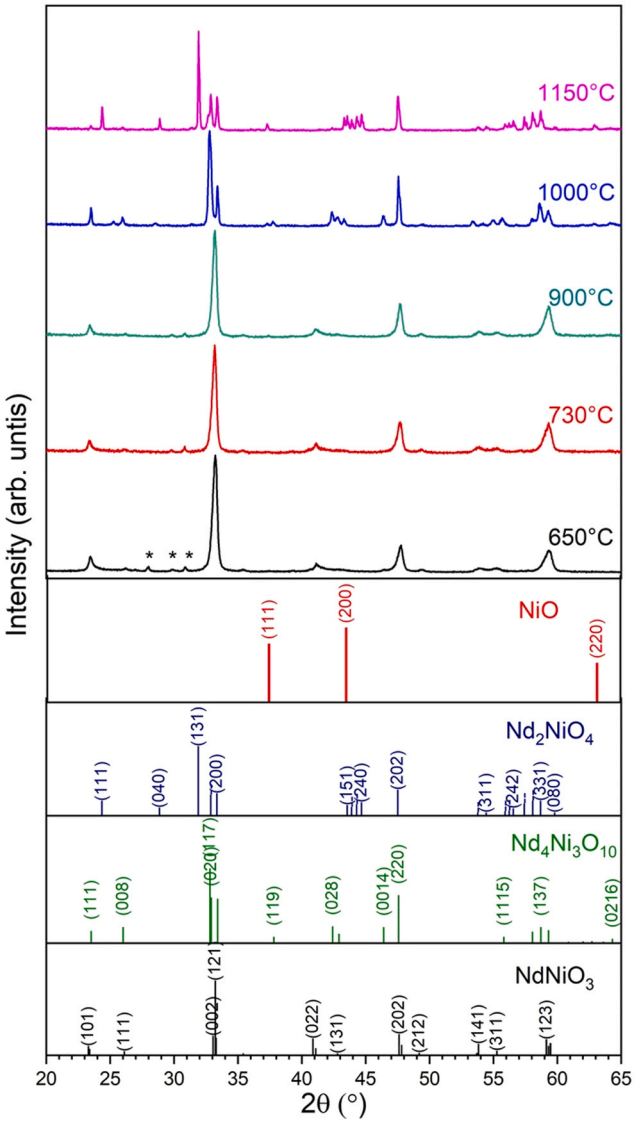

Fig. 4. The XRD patterns recorded at room conditions after annealing the samples at different temperatures in 1 bar of flowing O_2 for 12 h. It represents the decomposition of $NdNiO_3$. The JCPDS patterns of NiO, $NdNiO_3$, $Nd_4Ni_3O_{10}$ and Nd_2NiO_4 are shown at the bottom panels of the graph for comparison. The two secondary phases of hexagonal and cubic Nd_2O_3 are marked by (*).

will emerge.

3.3. Decomposition kinetics of $NdNiO_3$

After thermal stability of the different chemical phases at 1 bar of O_2 pressure during synthesis had been studied, the kinetics of $NdNiO_3$ decomposition at 950 °C was analysed according to Eq. (1). Fig. 6 shows the room temperature XRD patterns of the samples, obtained at 900 °C and at 950 °C after annealing treatment at increasing time intervals. According to Eq. (1), the same molar percentage of $Nd_4Ni_3O_{10}$ and NiO phases is expected to occur upon the decomposition of $NdNiO_3$. Fig. 7 shows the molar fraction of $NdNiO_3$, $Nd_4Ni_3O_{10}$ and NiO as a function of annealing time, at 950 °C. As annealing time increases, the molar percentage of $NdNiO_3$ phase decreases, unlike that of $Nd_4Ni_3O_{10}$ and NiO phases, which increases towards the equilibrium state after 132 h. However, as shown in Fig. 7, the molar percentage of NiO is somewhat smaller than that of $Nd_4Ni_3O_{10}$ phase, due to the very high volume of the $Nd_4Ni_3O_{10}$ lattice and high molar mass, contrasting with the low values for NiO. The volume percentage of NiO phase calculated by Rietveld

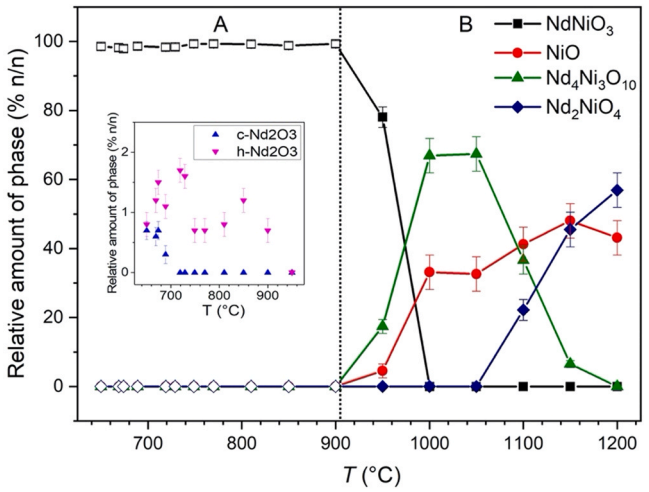

Fig. 5. Room temperature relative amounts (in molar percentage) of the sample as function of the annealing temperature. Results from Rietveld refinement converted to molar percent of each phase. The inset shows the mole percentage of cubic and hexagonal Nd_2O_3 impurities observed. Each point represents the mole percent of each phase after the sample had been exposed to a fixed temperature in 1 bar of flowing O_2 for 12 h.

refinement is therefore low (4.2% (v/v)) after 252 h, (see Fig. S3 in Supplemental material), leading to high uncertainties in the molar percentages.

3.4. Raman scattering, resistivity studies and XPS analysis

In order to further characterise the phases identified by XRD refinement, we have also performed micro-Raman spectroscopic studies. Fig. 8 shows representative unpolarised room temperature Raman spectra for samples annealed at 650 °C, 1050 °C and 1200 °C, respectively. As it was concluded from the XRD studies, the Raman spectroscopy data also evidence the emergence of different chemical phases for annealing temperatures above 900 °C. The Raman spectrum of the sample annealed at 650 °C matches the *Pnma* $NdNiO_3$ phase very well as reported in the literature [19,20]. However, to the best of our knowledge, there are no prior reports on Raman studies regarding $Nd_4Ni_3O_{10}$ and Nd_2NiO_4. Thus, we use the phase identification from XRD refinements to establish the first Raman signature of these compounds. Table 2 presents the wavenumber of the most intense modes of these compounds obtained from the analysis of the experimental spectra. Figs. S4 and S5 in Section S4 of Supplemental material show representative examples of the best fit of a sum of damped oscillators to the experimental spectra.

The Raman spectrum of the sample annealed at 1050 °C differs in the relative intensities of the bands when compared with the spectrum of the sample annealed at 650 °C; namely the bands around 180, 348 and 470 cm^{-1} have a significant increase of their intensity. This sample has 67%(n/n) of $Nd_4Ni_3O_{10}$ and 33%(n/n) of NiO (Fig. 6). Nevertheless, no Raman signature of the latter compound was found [21], because it corresponds only to 4% (v/v), indicating the studied grains are mostly from $Nd_4Ni_3O_{10}$ phase.

On the contrary, the sample annealed at 1200 °C exhibits a completely different Raman spectrum, mainly characterised by three broad bands. This sample has 57%(n/n) of Nd_2NiO_4 and 43%(n/n) of NiO (Fig. 6), but, as in the sample annealed at 1050 °C, no Raman signature of the latter compound was found [21]. Nd_2NiO_4 grains were preferentially chosen for measuring the spectra, therefore, the Raman spectra mainly involve the this phase.

Since the electrical properties strongly depend on both oxygen non-stoichiometry and Ni oxidation states, we studied the temperature dependence of the resistivity of the samples referred to above. The

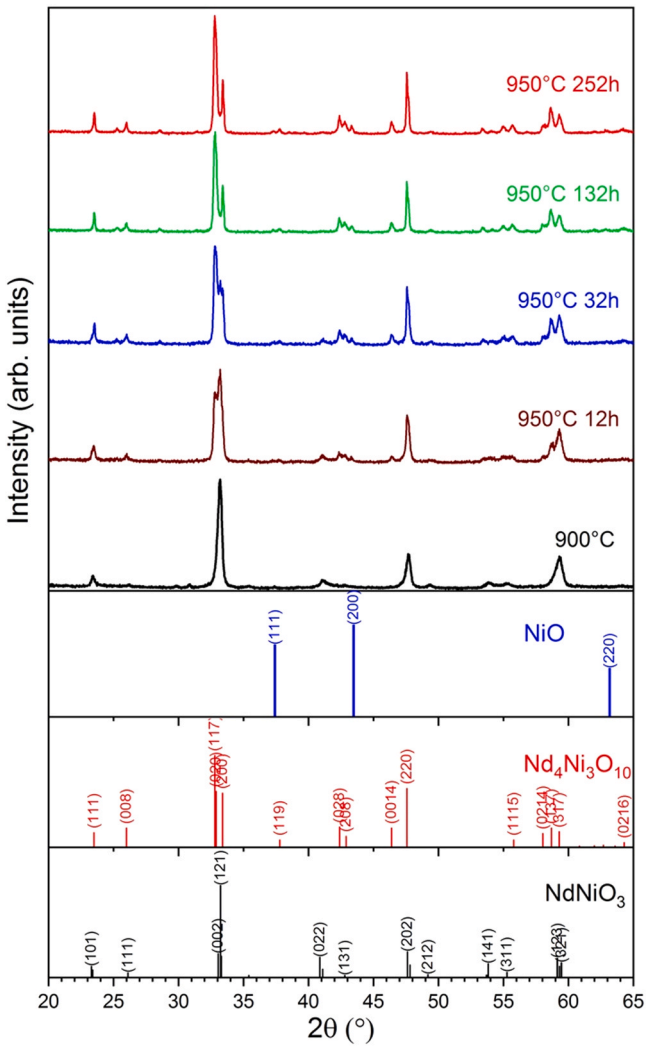

Fig. 6. XRD patterns representing the decomposition of $NdNiO_3$ at 950 °C in 1 bar of flowing O_2 as a function of time. For comparison, JCPDS patterns of NiO, $NdNiO_3$ and $Nd_4Ni_3O_{10}$ are shown at the bottom of the figure.

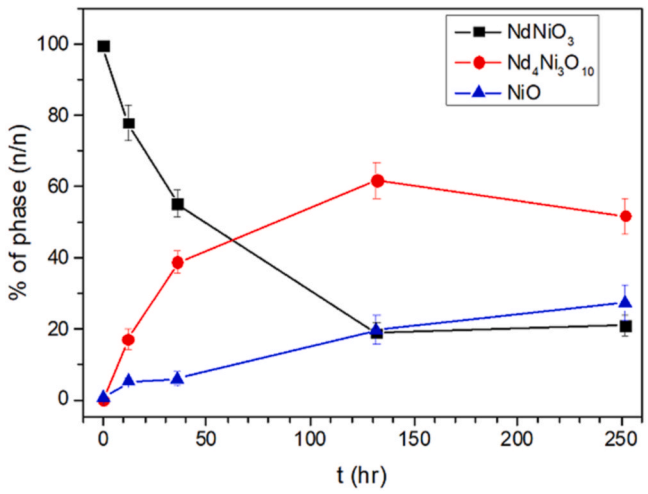

Fig. 7. Room temperature relative amounts (in molar percentage) of the sample as a function of total annealing time at 950 °C.

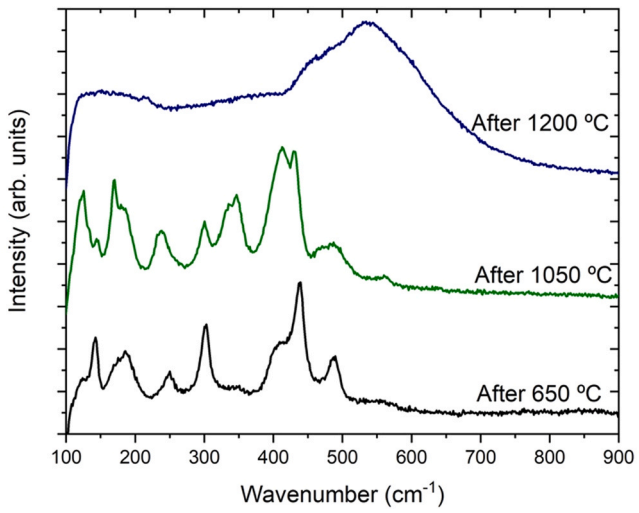

Fig. 8. Room temperature Raman spectra of sample after being annealed at 650 °C, 1050 °C and 1200 °C.

Table 2
Wavenumber of most intense Raman modes, with their respective symmetry for $NdNiO_3$ from Ref. [22].

$NdNiO_3$		$Nd_4Ni_3O_{10}$	Nd_2NiO_4
Mode symmetry [22]	Wavenumber (cm^{-1})	Wavenumber (cm^{-1})	Wavenumber (cm^{-1})
Ag(2)	138		
B2g(2)	143	143	
–	169	169	
–	181	180	
		188	
B2g(3)	192	195	
		233	221
Ag(3)	245	242	
–	290		
Ag(5)	299	299	
		333	330
		348	380
–	401	410	
–	420		
B2g(5)	435	431	461
–	465	470	532
Ag(7)/B2g(6)	485	490	594

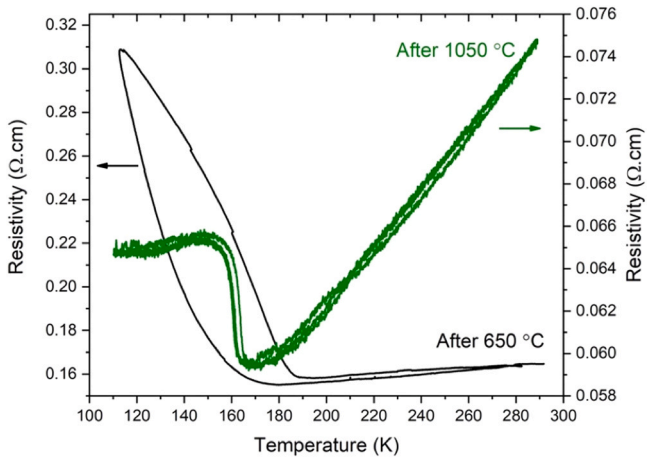

Fig. 9. Temperature dependence of the resistivity of sample after being annealed at 650 °C and 1050 °C.

obtained results are shown in Fig. 9.

The samples annealed at 650 and the 1050 °C exhibit the well-known metal-to-insulator transition at 158 K of the $NdNiO_3$ [19] and the metal-to-metal transition at 161 K of the $Nd_4Ni_3O_{10}$ respectively [23]. Considering the analysis of the effect of oxygen non-stoichiometry on the transport properties of $NdNiO_{3-\delta}$, addressed in the work of Nikulin et al. [10], we estimated a δ value of 0.09 ± 0.01 for our sample, based on the values of resistivity increase and thermal hysteresis at the MIT. A detailed explanation of this estimation is given in Section S5 of Supplemental material in Figs. S6 and S7. In order to confirm this value, we have also performed XPS analysis of the sample surface. Fig. S8 of Supplemental material shows the XPS spectra of the sample annealed at 650 °C, recorded at two different surface positions. A similar data analysis procedure was done as reported in Ref. [24]. For this, we have focused our attention on the Ni $2p_{3/2}$ energy peaks (details of data analysis is also presented in Supplemental material). We have calculated the percentage of Ni^{3+} and Ni^{2+} present in the sample (see Table S2) and the δ-value assuming the general formula $Nd^{3+}Ni^{3+}_{1-x}Ni^{2+}_{x}O_{3-\delta}$, which takes the value $\delta = 0.082 \pm 0.001$. It is worth to stress that XPS is a local superficial analytical technique, while the resistance measurement concerns the bulk properties. Despite the differences, the low oxygen vacancies concentration obtained from both techniques agrees very well, revealing a high oxygen stoichiometry of the $NdNiO_{3-\delta}$ phase, which fully validates the processing route proposed in this work. The amount of Ni^{2+} depends on the delta value. Concerning the mixed state valence, the average Ni oxidation state should be around 2.84. Since no electronic phase transitions for either Nd_2NiO_4 or NiO phases have been reported, resistivity measurements were not performed in this sample.

4. Conclusions

We have successfully synthesised $NdNiO_3$ samples by co-precipitation method followed by calcination at oxygen atmosphere, without resorting to any high-pressure synthesis techniques as reported in the literature. Thermal stability and decomposition kinetic studies of the samples were performed using XRD and the results were after confirmed by Raman spectroscopy, and resistivity measurements. Rietveld refinement of room temperature XRD patterns reveals that the $NdNiO_3$ phase is stable in samples annealed at temperatures up to 900 °C. At 950 °C, this phase decomposes into NiO and $Nd_4Ni_3O_{10}$ phases. An equilibrium state of this decomposition is obtained at 950 °C after 250 h, which allows one to conclude that, at this temperature, they should be in a peritectoid equilibrium. In turn, the $Nd_4Ni_3O_{10}$ phase decomposes at 1100 °C, above which the Nd_2NiO_4 phase is stabilised.

The Raman study fully confirms the XRD results, clearly corroborating the thermal stability of the different phases as the annealing temperature is being changed. Moreover, the Raman study carried out in this work also yields unprecedently reported Raman spectra of $Nd_4Ni_3O_{10}$ and Nd_2NiO_4 compounds. The temperature dependence of the resistivity of the sample annealed at 650 °C and at 1050 °C yields distinguishable fingerprint signatures of $NdNiO_3$ and $Nd_4Ni_3O_{10}$. The comparison between the resistivity results obtained for the sample annealed at 650 °C and others previously reported, along with a XPS analysis, have enabled an estimation of a $NdNiO_{3-\delta}$ phase with a $\delta = 0.082 \pm 0.001$. This particularly low value of δ, revealing a high oxygen stoichiometry of the obtained $NdNiO_{3-\delta}$ phase, fully validates the adequacy of the processing route proposed in this work to produce high quality $NdNiO_3$ ceramics. Ergo, it may be most efficiently used for large target production, and application in thin film device deposition techniques.

CRediT authorship contribution statement

A.A. Bassou: Investigation, Data curation, Formal analysis, Writing – original draft, Writing – review & editing. **P. Machado:** Data curation, Writing – review & editing. **M.M. Gomes:** Investigation, Data curation,

Formal analysis, Writing – review & editing. **B. Manjunath:** Investigation, Data curation, Formal analysis, Writing – review & editing. **R. Vilarinho:** Data curation, Formal analysis, Writing – review & editing. **B. Silva:** Data curation, Writing – review & editing. **J. Oliveira:** Data curation, Writing – review & editing. **B. Almeida:** Funding acquisition, Project administration, Writing – review & editing. **A. Almeida:** Writing – review & editing. **L.S. Fernandes:** Investigation, Data curation, Formal analysis, Writing – review & editing. **J.R. Fernandes:** Resources, Software, Writing – review & editing. **J. Agostinho Moreira:** Funding acquisition, Project administration, Methodology, Writing – review & editing. **P.B. Tavares:** Funding acquisition, Project administration, Methodology, Investigation, Formal analysis, Writing – original draft, Writing – review & editing.

Declaration of Competing Interest

The authors declare that they have no known competing financial interests or personal relationships that could have appeared to influence the work reported in this paper.

Acknowledgements

The authors would like to acknowledge Fundação para a Ciência e Tecnologia (FCT) through projects NORTE/01/0145/FEDER/028538, CERN/FIS-PAR/0005/2017, CERN/FIS-TEC/0003/2019, PTDC/FIS-MAC/29454/2017 and when appropriate co-financed by FEDER under PT2020 Partnership Agreement: CQVR: UIDB/QUI/00616/2020; IFIMUP-IN: Norte-070124-FEDER-000070; NECL: NORTE-01-0145-FEDER-022096, UID/NAN/50024/2019. P. Machado and J. Oliveira acknowledge FCT through Ph.D. Grants SFRH/BD/108509/2015 and SFRH/BD/146886/2019 respectively. A special acknowledgment is made to CEMUP for XPS measurements.

Declaration of interest statement

The authors declare that they have no known competing financial interests or personal relationshipsthat could have appeared to influence the work reported in this paper.

Appendix A. Supplementary Material

Supplementary data associated with this article can be found in the online version at doi:10.1016/j.mtcomm.2021.102663.

References

[1] P. Zubko, S. Gariglio, M. Gabay, P. Ghosez, J.-M. Triscone, Interface physics in complex oxide heterostructures, Annu. Rev. Condens. Matter Phys. 2 (2011) 141–165, https://doi.org/10.1146/annurev-conmatphys-062910-140445.

[2] Y. Tokura, Orbital physics in transition-metal oxides, Science 288 (2000) 462–468, https://doi.org/10.1126/science.288.5465.462 (80–.).

[3] B. Torriss, J. Margot, M. Chaker, Metal-insulator transition of strained $SmNiO_3$ thin films: structural, electrical and optical properties, Sci. Rep. 7 (2017) 1–9, https://doi.org/10.1038/srep40915.

[4] S. Heo, C. Oh, J. Son, H.M. Jang, Influence of tensile-strain-induced oxygen deficiency on metal-insulator transitions in $NdNiO_{3-\delta}$ epitaxial thin films, Sci. Rep. 7 (2017) 1–9, https://doi.org/10.1038/s41598-017-04884-2.

[5] J. Varignon, M.N. Grisolia, J. Íñiguez, A. Barthélémy, M. Bibes, Complete phase diagram of rare-earth nickelates from first-principles, npj Quantum Mater. 2 (2017) 1–8, https://doi.org/10.1038/s41535-017-0024-9.

[6] G. Catalan, Progress in perovskite nickelate research, Phase Transit. 81 (2008) 729–749, https://doi.org/10.1080/01411590801992463.

[7] J. Torrance, P. Lacorre, A. Nazzal, E. Ansaldo, C. Niedermayer, Systematic study of insulator-metal transitions in perovskites $RNiO_3$ (R=Pr,Nd,Sm,Eu) due to closing of charge-transfer gap, Phys. Rev. B 45 (1992) 8209–8212, https://doi.org/10.1103/PhysRevB.45.8209.

[8] J.A. Alonso, M.J. Martínez-Lope, M.T. Casais, M.A.G. Aranda, M.T. Fernández-Díaz, Metal–insulator transitions, structural and microstructural evolution of $RNiO_3$ (R = Sm, Eu, Gd, Dy, Ho, Y) perovskites: evidence for room-temperature charge disproportionation in monoclinic $HoNiO_3$ and $YNiO_3$, J. Am. Chem. Soc. 121 (1999) 4754–4762, https://doi.org/10.1021/ja984015x.

[9] P. Lacorre, J. Pannetier, S.A.I. Nazzal, P.W. Wang, T.C. Huang, Synthesis, crystal structure and properties of metalic $PrNiO_3$: comparison with metallic $NdNiO_3$ and semiconducting $SmNiO_3$, J. Solid State Chem. 91 (1991) 225–237.

[10] I.V. Nikulin, M.A. Novojilov, A.R. Kaul, S.N. Mudretsova, S.V. Kondrashov, Oxygen nonstoichiometry of $NdNiO_{3-\delta}$ and $SmNiO_{3-\delta}$, Mater. Res. Bull. 39 (2004) 775–791, https://doi.org/10.1016/j.materresbull.2004.02.005.

[11] J.K. Vassiliou, M. Hornbostel, R. Ziebarth, F.J. Disalvo, Synthesis and properties of $NdNiO_3$ prepared by low-temperature methods, J. Solid State Chem. 81 (1989) 208–216, https://doi.org/10.1016/0022-4596(89)90008-X.

[12] M.K. Hooda, C.S. Yadav, Electronic properties and the nature of metal-insulator transition in $NdNiO_3$ prepared at ambient oxygen pressure, Phys. B Condens. Matter 491 (2016) 31–36, https://doi.org/10.1016/j.physb.2016.03.014.

[13] N.W. Medendorp, D.R. Gaskell, Phase stability and microstructural evolution in the system $Bi_2Sr_2CaCu_2O_{8+x}$, J. Am. Ceram. Soc. 82 (1999) 2209–2218, https://doi.org/10.1111/j.1151-2916.1999.tb02064.x.

[14] J.Agostinho Moreira, A. Almeida, M.R. Chaves, M.L. Santos, P.P. Alferes, I. Gregora, Raman spectroscopic study of the phase transitions and pseudospin phonon coupling in sodium ammonium sulphate dihydrate, Phys. Rev. B 76 (2007), 174102, https://doi.org/10.1103/PhysRevB.76.174102.

[15] H. Mueller-Buschbaum, Zur Struktur der A-Form der Sesquioxide der Seltenen Erden. II Strukturuntersuchung an Nd_2O_3, Z. Anorg. Allg. Chem. 343 (1966) 6–10.

[16] H. Bommer, Die Gitterkonstanten der C-Formen der Oxyde der seltenen Erdmetalle, Z. Anorg. Allg. Chem. 241 (1939) 273–280, https://doi.org/10.1002/zaac.19392410215.

[17] U. Lehmann, H. Mueller-Buschbaum, Der Aufbau von Nd_2NiO_4 und seine Verwandtschaft zu La_2NiO_4 und La_2CuO_4, Z. Naturforsch. Teil B Anorg. Chem. Org. Chem. 35 (1980) 389–390.

[18] A. Olafsen, H. Fjellvåg, B.C. Hauback, Crystal structure and properties of $Nd_4Co_3O_{(10+\delta)}$ and $Nd_4Ni_3O_{(10-\delta)}$, J. Solid State Chem. 151 (2000) 46–55, https://doi.org/10.1006/jssc.2000.8620.

[19] C. Girardot, J. Kreisel, S. Pignard, N. Caillault, F. Weiss, Raman scattering investigation across the magnetic and metal-insulator transition in rare earth nickelate R NiO_3 (R=Sm, Nd) thin films, Phys. Rev. B Condens. Matter Mater. Phys. 78 (2008) 1–7, https://doi.org/10.1103/PhysRevB.78.104101.

[20] M. Zaghrioui, A. Bulou, P. Lacorre, P. Laffez, Electron diffraction and Raman scattering evidence of a symmetry breaking at the metal-insulator transition of $NdNiO_3$, Phys. Rev. B Condens. Matter Mater. Phys. 64 (2001) 811021–811024, https://doi.org/10.1103/PhysRevB.64.081102.

[21] N. Mironova-Ulmane, A. Kuzmin, I. Steins, J. Grabis, I. Sildos, M. Pärs, Raman scattering in nanosized nickel oxide NiO, J. Phys. Conf. Ser. 93 (2007) 8–13, https://doi.org/10.1088/1742-6596/93/1/012039.

[22] H.C. Gupta, M.K. Singh, L.M. Tiwari, A lattice dynamical investigation of Raman and infrared wavenumbers at the zone center of the orthorhombic $NdNiO_3$ perovskite, J. Phys. Chem. Solids 64 (2003) 531–533, https://doi.org/10.1016/S0022-3697(02)00336-0.

[23] B.-Z. Li, C. Wang, P.T. Yang, J.P. Sun, Y.-B. Liu, J. Wu, Z. Ren, J.-G. Cheng, G.-M. Zhang, G.-H. Cao, Metal-to-Metal Transition and Heavy-Electron State in $Nd_4Ni_3O_{10\text{-delta}}$, 2020, pp. 1–10. ⟨http://arxiv.org/abs/2001.09059⟩.

[24] C. Hu, X. Wang, T. Yao, T. Gao, J. Han, X. Zhang, Y. Zhang, P. Xu, B. Song, Enhanced electrocatalytic oxygen evolution activity by tuning both the oxygen vacancy and orbital occupancy of B-site metal cation in $NdNiO_3$, Adv. Funct. Mater. 29 (2019), 1902449, https://doi.org/10.1002/adfm.201902449.